JOURNAL OF AIRCRAFT
Vol. 45, No. 6, November–December 2008

Topology Optimization Approach for the Determination of the Multiple-Configuration Morphing Wing Structure

Daisaku Inoyama*
University of Dayton, Dayton, Ohio 45469
Brian P. Sanders†
U.S. Air Force Research Laboratory, Wright–Patterson Air Force Base, Ohio 45433
and
James J. Joo‡
University of Dayton Research Institute, Dayton, Ohio 45469

DOI: 10.2514/1.29988

The paper introduces an innovative topology optimization approach for determining the distribution of structural properties and actuators to design a morphing wing that is capable of achieving multiple target shapes. The previous investigation by the authors demonstrated, using various problem formulations and a novel modeling concept, the fundamental topology synthesis of a simple two-configuration morphing wing structure. The primary objective of the present investigation is therefore to introduce improvements and extensions to the previous concepts and problem formulations to those capable of accommodating the multiple-configuration definitions. The investigation includes the formulation of appropriate topology optimization problems and the development of effective modeling concepts. In addition, principal issues on the external load dependency and the reversibility of a design, as well as the appropriate selection of a reference configuration, are addressed in the investigation. The methodology to control actuator distributions and concentrations is also discussed. Finally, an example multiple-configuration problem that portrays the generic surveillance mission is solved to demonstrate the potential capabilities of the approach.

Nomenclature

A	=	actuator set
A_i	=	subset of the actuator set that corresponds to the ith configuration
B	=	attachment set
$E_m^{(i)}$, $E_{\max}^{(i)}$	=	squared axial stroke length and stroke limit of the mth line element for the ith configuration
$\mathbf{F}$	=	global load vector
$\mathbf{F}_{\text{ext}}^{(i)}$	=	external load vector for the ith configuration
$\mathbf{F}_j^{0}$	=	rated force vector of the jth actuator
J	=	joint set
$\mathbf{K}$	=	global stiffness matrix
$\mathbf{K}_i^{(\text{AX})}$, $\mathbf{K}_i^{(\text{NAX})}$	=	axial and nonaxial stiffness matrices of the ith line element
$\mathbf{K}_{(i)}^{(R)}$, $\mathbf{K}_i^{(\text{NR})}$	=	rotational and nonrotational stiffness matrices of the ith joint element
$\mathbf{K}_i^{(S)}$, $\mathbf{K}_i^{(\text{NS})}$	=	sliding and nonsliding stiffness matrices of the ith attachment element
$\mathbf{K}_{\text{skin}}$	=	simulated flexible-skin stiffness matrix
L	=	line set
$L1$, $L2$	=	subsets of a line set
N_F	=	total number of fixed attachments allowed in the solution
N_{shape}	=	total number of target shapes in the problem
N_{tgt}	=	total number of target degrees of freedom at the morphing boundary
N_Ω, N_Φ	=	total number of line-element and actuator locations in the model
tgt	=	target-degree-of-freedom set
$T_j^{(i)}$, $U_j^{(i)}$	=	target and actual displacements for the ith configuration at the jth target degree of freedom
$\mathbf{U}^{(i)}$	=	vector of actual displacements for the ith configuration
$V_{\max}$, $V_{\min}$	=	maximum and minimum allowable volume
$W_S^{(i)}$, $W_A^{(i)}$	=	shape and actuator weight/scale constants for the ith configuration
β, p, α	=	penalty constants for joint, line, and attachment variables
$\varepsilon_{\max}$	=	maximum allowable target-degree-of-freedom displacement error
$\boldsymbol{\rho}$, ρ_j	=	vector of design variables and its jth components in the set
$\rho_{\min}$	=	minimum value of design variables
Ω_i, Φ_i	=	set of coincident line-element and actuator variables at the ith location

Presented as Paper 1712 at the 48th AIAA/ASME/ASCE/AHS/ASC Structures, Structural Dynamics, and Materials Conference, Honolulu, HI, 23–26 April 2007; received 24 January 2007; revision received 29 April 2008; accepted for publication 7 June 2008.

*Currently Senior Engineer, Space Systems Group, Orbital Sciences Corporation, 21839 Atlantic Boulevard, Dulles, VA 20166.

†Senior Research Scientist, Air Vehicles Directorate. Associate Fellow AIAA.

‡Research Engineer, Aerospace Mechanics Division. Member AIAA.

I. Introduction

SHAPE-ADAPTIVE capability in air vehicles may be highly desirable for numerous reasons. First and foremost, such a capability can potentially dramatically increase aircraft flight performance and efficiency while attempting the operation across a broad envelope of flight conditions. The ability to continuously transform vehicle geometry provides a single air vehicle with a multiple-mission capacity, as it enables the vehicle to maintain and operate within the optimum or near-optimum flight envelope, even as underlying flight dynamics may vary radically from mission to mission or segment to segment within a mission. The Mission Adaptive Wing (MAW) program is one of the first flight-test initiatives to attempt such an active control of wing geometries [1,2]. The concept involves four conventional control surfaces with a

reduced flexible wing to control spanwise twists. Although MAW programs demonstrated the technological feasibility and the potential benefits of shape adaptation in air vehicles, the practicality and the balance between benefits and system sophistications still remain as a major obstacle. The actuation system (i.e., the combination of structure, mechanism, and actuators) must be designed effectively to avoid adaptation costs to displace potential benefits.

Topology optimization of a morphing mechanism is not a simple task, often involving simultaneous solutions of multidisciplinary problems with a large number of optimization variables. In spite of its complexity, design methodology based on topology optimization may be ideal for the present investigation due to its capability to determine the optimum system configuration without well-defined initial conditions. For an application to morphing-air-vehicle design, the complexity of multidisciplinary topology optimization can be further exacerbated by large structural displacements and rigid-body motions that arise from shape adaptations. The potential benefit of a topology optimization methodology as a mechanism design tool, in general, is well depicted in the study by Pedersen et al. [3]. The research describes the topology synthesis of a large-displacement compliant mechanism using nonlinear finite element analysis. In addition, the research explains a solution procedure for path generation problems. A more recent study [4] demonstrates the topology optimization process for a design of path-generating articulated mechanisms. Though these investigations cover the general aspect of path generation procedures, the concept may possess close relationships, including its multi-objective nature, to the design of morphing-air-vehicle structures.

The potential effectiveness of optimization techniques in the design of a morphing air vehicle with multiple design points and criteria is demonstrated in few notable investigations [5,6]. One of the investigations demonstrates the topology optimization methodology for the design of a compliant mechanism for an airfoil shape adaptation [5]. The study involves the determination of an optimum airfoil shape and the corresponding mechanism topology, as well as actuator placements, to adapt the original shape to the determined optimum shape. The researchers present both solutions of coupled simultaneous (involving coupled fluid–structure analysis) and decoupled two-step approaches. Another notable investigation [6] addresses the multiple-objective nature of an optimization process for the design of morphing air vehicles at multiple configurations. The investigation involves the performance optimization of a buckled-wing morphing air vehicle at its fused and parted configurations. The design variables that define various airfoil shapes of the fused state and the parting line for two buckled airfoils are optimized to maximize the lift-to-drag ratio of the fused state and the lift coefficient of the buckled airfoils. The researchers demonstrate both multiple steps and simultaneous approaches to solve the optimization problem. Though the preceding investigations do not consider a mechanism design that is capable of achieving multiple shapes or configurations, they provide excellent illustrations of how optimization techniques can be applied to the conceptual design of a morphing air vehicle.

Among few recent investigations [7–10] that address the mechanization aspect of a morphing aircraft structure, one investigation presents an innovative structural concept based on tendon-actuated compliant cellular trusses [7]. The modeling concept includes the lattice of cells constructed of truss members and compliant joints, actuated by pulling and/or releasing cables or tendons within each cell. The main feature of this concept is that by controlling the appropriate tendons, the cells can be made to behave as a compliant mechanism locally and temporarily. Researchers demonstrate that the collective local behaviors of each individual cell can be translated to a large-scale global shape change. In addition, considerations are given to the more detailed aspects of the concept, such as cell sizing and geometry, structural strength and weight, and potential skin designs. The subsequent investigation [8] involves the formulation and solution of a topology optimization problem to optimally place tendons and trusses using a specialized genetic algorithm (GA).

The previous investigation [10] by the authors demonstrated the potential capability of a topology optimization methodology for the determination of distributed actuation systems for in-plane morphing structures. The investigation introduces the fundamental modeling concept, various topology optimization formulations, and solution procedures for a two-configuration in-plane morphing wing structure with simulated flexible-skin elements. Though the basic concept and formulations cover all the fundamental requirements of a morphing wing, the study lacks the consideration to accommodate the multiple-shape-changing definition that is one of the most desirable capabilities of a morphing air vehicle. Moreover, the investigation introduced a novel approach in the design of morphing structures through an optimization technique, but the problem formulation is rather imprecise and did not contain clear definitions to accommodate more specific conditions that are applicable to morphing structures, such as reversibility and external-load-dependent issues.

Over the past decade, numerous investigations have been conducted for morphing mechanism design, topology optimization technique, actuator placement, and system efficiency separately [9,11–20], but very little attention has been given to the combination of these disciplines. Therefore, the work here aims to develop a computational design approach that is capable of achieving efficient integration of actuators, mechanisms, and elastic structures for the design of a multiple-configuration morphing-air-vehicle structure. More specifically, the main focus of the investigation is to explore the potential benefit of optimization techniques as a design tool for the determination of actuation systems that minimize the total actuator usage while achieving the desired structural shapes. The investigation involves the extension of the concept and problem formulations developed in the previous investigation [10] to those capable of accommodating the multiple-configuration definitions.

II. General Procedure and Technical Approach

A. Analysis Model Concept

The analysis model concept used in this investigation is nearly identical to that introduced in the previous investigation [10] by the authors. In other words, the model contains all the components and element configuration definitions that were previously introduced. As the understanding of model descriptions and its characteristics is essential to the discussions in the subsequent sections of this paper, they are briefly explained here for purposes of review.

The in-plane morphing wing model used in the investigation consists of a lattice of cells that contain definitions of joint, line, and attachment elements, as shown in Fig. 1a. Each line element assumes an appropriate configuration corresponding to the value of design variables that are determined by the optimization process. Line elements in the model can be frames, trusses, telescoping members, or actuators, as shown in Fig. 1b. Frame elements are conventional finite elements with axial and bending stiffnesses. Truss elements are the decompositions of frame elements and consist only of axial stiffness. Though the physical distinction between trusses and frames often does not exist, load-bearing characteristics of the structure may be revealed by observing the topology or the layout of these elements.

Telescoping members are classified into two categories: either active or inactive. Inactive telescopes are prismatic elements that have very low axial stiffness with beam-bending stiffness and are not capable of delivering an actuation force. Whenever a telescoping member has an associated actuation force, the element is classified as an active telescope. An actuator is simply an element with equal and opposite nodal forces at its nodes and is not intended to resist any loads through its physical stiffness. Both telescoping members and actuators have axial stroke limits that prohibit them from extending more than a predefined length, thereby preventing these elements from having unrealistically large strokes. In addition, actuator forces must be limited to a certain predefined value. Whenever very low stiffness is present in all degrees of freedom, the element is considered as structurally or mechanically noncontributing and selected to be nonexistent or void.

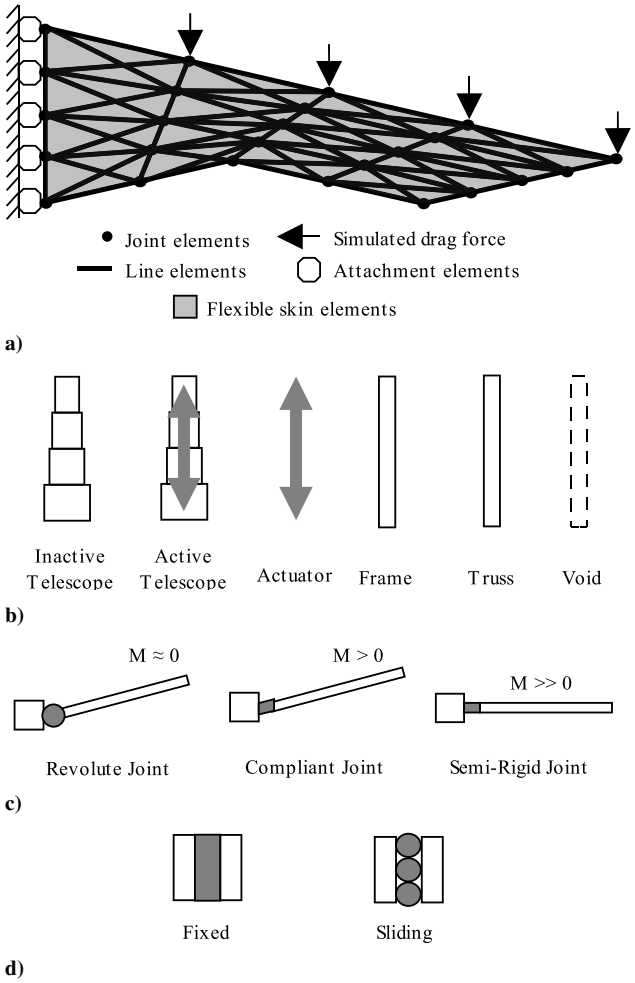

Fig. 1 Illustrations of : a) analysis model, b) line-element configuration, c) joint-element configuration, and d) attachment-element configuration.

Joint elements can be classified into the following types: revolute, compliant, or semirigid, as shown in Fig. 1c. Revolute joints can be considered as rotating hinges simulated by very low rotational stiffness and very high stiffness in all other directions. Accordingly, semirigid joints have very high stiffness in the rotational and all other directions. Compliant joints have intermediate rotational stiffness that can be physically interpreted as friction joints or high-strain joints. These joints are analogous to rotational springs. In addition to motions around these defined joints, rotations about truss elements are also possible, as in the case of implicitly defined pinned joints in truss structures.

Among several possible configurations for an attachment element, two primary ones, as shown in Fig. 1d, are considered in the model presented here. The sliding boundary condition allows corresponding attachments to slide in a single translational direction along a fuselage, which is numerically represented by very low stiffness in a sliding direction and very high stiffness in other directions. The fixed boundary condition prohibits any relative motions by very high stiffness in entire degrees of freedom. Whenever a fixed or sliding boundary condition is connected to the structure through a revolute or compliant joint, it can be regarded as a pinned or sliding revolute attachment, respectively.

The words *very low* and *very high* are relative to the full stiffness of a frame element. Therefore, rigid-body motions are the result of relatively soft elements and, at the same time, structural strains are carried to the load-resisting structure through relatively stiff elements. Evidently, very low and very high values must be chosen carefully to ensure numerical stabilities in computational procedures.

In addition to line, joint, and attachment elements, the model contains flexible-skin elements. As reliable representation of flexible morphing vehicle skin is not available at the moment, four node-displacement elements with very low membrane stiffness are applied over each cell to represent the flexible skin. Although the importance of a reliable skin model is well understood, the pillowing effect that arises from out-of-plane pressure loading is not a concern for the problem presented in this paper and therefore such a simple representation of flexible skin is considered to be sufficient.

This paper deals only with a linear finite element method scheme to keep the analysis at the conceptual level, but the preceding model should be equally applicable to geometrically or materially nonlinear finite element cases, in which stiffness and force boundary conditions are a function of displacements and rotations, with a significant increase in computational costs.

B. Basic Problem Formulation

One important aspect that must be considered in the topology problem formulation with a multiple-configuration definition is that a single structure must be capable of satisfying multiple target shapes. In such a problem formulation, the cost function will essentially be multi-objective. For instance, the weighted sum of shape error terms and actuator usage terms can be minimized to allow simultaneous satisfaction of shape achievement and actuator placement.

Minimize:

$$f_0(\boldsymbol{\rho}) = \sum_{i}^{N_{\text{shape}}} W_S^{(i)} \sum_{j \in \text{tgt}} \left(T_j^{(i)} - U(\boldsymbol{\rho})_j^{(i)} \right)^2 + \sum_{i}^{N_{\text{shape}}} W_A^{(i)} \sum_{j \in A_i} \rho_j \qquad (1)$$

The preceding multi-objective function contains shape error terms and actuator usage terms for each target configuration. The topology design variables $\boldsymbol{\rho}$ control the stiffness of corresponding line, joint, attachment, or actuator elements. The important point to note here is that the actual displacement vector for the ith target configuration is independent of actuator loads that do not correspond to that particular configuration (i.e., each target configuration is satisfied by its own load set). In addition, the displacements for all configurations are a function of the same structural and joint design variables, thereby not allowing interconfiguration variation in structural topology. In the objective function, the perfect-shape satisfaction is indicated when the difference between a target displacement ($T_j^{(i)}$) and an actual displacement ($U_j^{(i)}$) vanishes for all target degrees of freedom in every configuration. The square of each shape error term is necessary to ensure a positive quantity. The actuator usage term is simply a summation of entire actuator variables in every configuration. The relative importance of shape and actuator terms is controlled by weight/scale constants $W_S^{(i)}$ and $W_A^{(i)}$, respectively. It is intuitive that the shape objectives must dominate the problem, because the minimization of actuator usage can be considered as a secondary or less significant objective.

The topology optimization problem must include equilibrium constraints at multiple configurations. Therefore, the problem must contain a minimum of N_{shape} equilibrium conditions to be satisfied identically and simultaneously. In addition, the actuator definition is composed of N_{shape} load sets to represent various actuator loading conditions to attain N_{shape} configurations. The line-element stroke length must be constrained for each displacement set for the particular configuration to avoid unrealistically large actuator or telescope stroke length. The corresponding topology optimization problem can be written in the standard nonlinear programming form.

Minimize:

$$f_0(\boldsymbol{\rho}) \qquad (2)$$

Subject to:

$$\mathbf{K}\,\mathbf{U}^{(i)} = \mathbf{F}^{(i)} + \mathbf{F}_{\text{ext}}^{(i)} \qquad (3)$$

$$f_m^{(i)} = \mathrm{E}_m^{(i)} - \mathrm{E}_{\max}^{(i)} \leq 0 \qquad (4)$$

$$\sum_{i\in L1}\rho_i - V_{\max 1} \le 0 \tag{5}$$

$$\sum_{i\in L2}\rho_i - V_{\max 2} \le 0 \tag{6}$$

$$\sum_{i\in L1}\rho_i + \sum_{i\in L2}\rho_i - V_{\max} \le 0 \tag{7}$$

$$\sum_{j\in A_i}\rho_j - A^{(i)}_{\max} \le 0 \tag{8}$$

$$\sum_{j\in A}\rho_j - A_{\max} \le 0 \tag{9}$$

$$\sum_{i\in B}\rho_i - N_F \le 0 \tag{10}$$

$$\rho_{\min} \le \boldsymbol{\rho} \le 1.0 \tag{11}$$

where

$$\mathbf{K} = \sum_{i\in J}\left(\rho_i^{\beta}\mathbf{K}_i^{(R)} + \mathbf{K}_i^{(\mathrm{NR})}\right) + \sum_{i\in L1}\left(\rho_i^{p}\mathbf{K}_i^{(\mathrm{AX})}\right) + \sum_{i\in L2}\left(\rho_i^{p}\mathbf{K}_i^{(\mathrm{NAX})}\right) + \sum_{i\in B}\left(\rho_i^{\alpha}K_i^{(S)} + \mathbf{K}_i^{(\mathrm{NS})}\right) + \mathbf{K}_{\mathrm{skin}} \tag{12}$$

$$\mathbf{F}^{(i)} = \sum_{j\in A_i}\rho_j\mathbf{F}^0 + \mathbf{F}_{\mathrm{ext}} \tag{13}$$

The superscript i runs from 1 to the total number of target configurations, denoting the multiple of conditions that must be satisfied. The volume constraints (5–7) do not contain the superscript because there is no interconfiguration variation in the structure. Yet the multiple expressions for volume constraint indicate that the volume of each structural component, as well as the total volume, should be constrained individually to prevent excessive use of a single component. The maximum actuator usage values $A^{(i)}$ and A_T limit the actual actuator usage to the certain allowable values and are intra- and interconfiguration quantities, respectively. The attachment constraint is applied to limit the number of fixed attachments in a solution. Finally, side constraints are applied to design variables as in the standard topology optimization problem, in which design variables are allowed to vary from a small positive number $\rho_{\min}$ to a unity.

In the formulation, one may notice that actuator variables are unidirectional due to the positive value requirement placed by side constraints (11). If the bidirectional characteristic of actuators is desired, a natural choice is to apply two opposing actuator variables to each potential actuator location. The contradiction in these coincident design variables should not be a concern, as such a condition is seen as inefficient or expensive by the actuator usage minimization term in the objective function. Another possible bidirectional implementation is to use squared actuator variables with negative lower bounds. Though the technique involves only a single actuator variable per actuator, the squared sum of actuator variables in the objective and/or constraint functions can possibly create artificial actuator distributions due to the false numerical advantage that the sum of products of fractions may present.

The objective function (1) can be reduced in terms by setting a set of weight constants to zero. Two separate problem formulations can be devised: shape error and actuator usage minimization formulations. For instance, the problem can be solved using only the shape objective by setting the actuator weights to zero. This shape error minimization problem can be solved by specifying the desired value of actuator usage as a constraint. The primary disadvantage of this formulation is that the desired value of actuator usage for each configuration must be known a priori, although these usage values are often difficult to predict. Additionally, because the actuator variables are not minimized in this case, opposing/coinciding actuator variables may become coexistent if the maximum actuator usage values are improperly assigned.

The actuator minimization problem results when weighting factors for the shape terms are set to zero. For this case, one may apply the following shape constraint in addition to Eqs. (3–9):

$$\left(T_j^{(i)} - U_j^{(i)}\right)^2 - \varepsilon^2_{\max} \le 0 \qquad i = 1,\ldots,N_{\mathrm{shape}} \quad j = 1,\ldots,N_{\mathrm{tgt}} \tag{14}$$

This shape constraint defines target shapes by constraining the target degrees of freedom along the morphing boundary within a certain error $\varepsilon_{\max}$. In other words, the target shape is defined using a constraint that effectively applies a cage or a target-error limitation around each target point, although such a constraint generally creates a rather large constraint violation at the initial iteration in the optimization process. To avoid this large constraint violation, one may solve the shape error minimization problem first and then solve the actuator minimization problem. The potential benefit of such a sequential solution procedure is discussed in the previous investigation [10] by the authors. In addition, one should remember that the constraint (14) introduces N_{shape} times N_{tgt} constraints to be satisfied, and therefore the problem may become excessively complex for some optimization techniques to solve if the morphing boundary contains numerous target points.

The sensitivity of the objective function can be obtained analytically using the adjoint method, in which the static equilibrium condition (10) is implicitly satisfied upon computation of sensitivities:

$$\frac{\partial f_0}{\partial \rho_e} = 2\sum_{i=1}^{N_{\mathrm{shape}}} W_s^{(i)} \sum_{j\in\mathrm{tgt}}\left[\left(T_j^{(i)} - U_j^{(i)}\right)\mathbf{a}_j^T\frac{\partial \mathbf{K}}{\partial \rho_e}\mathbf{U}^{(i)}\right] \qquad e \in J, L1, L2, B \tag{15}$$

$$\frac{\partial f_0}{\partial \rho_e} = -2W_S^{(i)} \sum_{j\in\mathrm{tgt}}\left[\left(T_j^{(i)} - U_j^{(i)}\right)\mathbf{a}_j^T\frac{\partial \mathbf{F}^{(i)}}{\partial \rho_e}\right] - W_A^{(i)} \qquad e \in A_i \tag{16}$$

where $\mathbf{a}_j$ is the solution of adjoint state problem for the jth target degree of freedom:

$$\mathbf{K}\,\mathbf{a}_j = \mathbf{l}_j \tag{17}$$

where $\mathbf{l}_j$ is the unit vector defined by a displacement of the jth degree of freedom for the ith configuration:

$$U_j^{(i)} = \mathbf{l}_j^T\mathbf{U}^{(i)} \tag{18}$$

The sensitivities of stroke-limit constraint can also be obtained analytically:

$$\frac{\partial f_m^{(i)}}{\partial \rho_e} = -2\boldsymbol{\Psi}_m^T\mathbf{U}^{(i)}\boldsymbol{\Lambda}_m^T\frac{\partial \mathbf{K}}{\partial \rho_e}\mathbf{U}^{(i)} \qquad e \in J, L1, L2, B \tag{19}$$

$$\frac{\partial f_m^{(i)}}{\partial \rho_e} = 2\boldsymbol{\Psi}_m^T\mathbf{U}^{(i)}\boldsymbol{\Lambda}_m^T\frac{\partial \mathbf{F}^{(i)}}{\partial \rho_e} \qquad e \in A_i \tag{20}$$

where $\mathbf{\Lambda}_m$ is obtained from solving the following system:

$$\mathbf{K}\,\mathbf{\Lambda}_m = \mathbf{\Psi}_m \tag{21}$$

where $\mathbf{\Psi}_m$ is the rotational transformation vector that defines the direction of a line-element stroke:

$$E_m^{(i)} = \mathbf{\Psi}_m^T \mathbf{U}^{(i)} \tag{22}$$

For the actuator usage minimization problem, the sensitivities of shape constraints (14) must be obtained. Because the first term of the multi-objective function (1) is essentially the same as the shape constraint, the sensitivity will be identical to Eq. (15) for the structural variables. The sensitivity with respect to actuator variables will be identical to Eq. (16) without the second term. The sensitivities for other constraints (5–10) are straightforward and contain only ones and zeros.

One must note that the solution may be significantly influenced by a balance between shape error and actuator weight/scale constants. Therefore, it is imperative to analyze and understand the effect of these constants. The weight constants must be chosen based on consideration of the initial shape errors and the actuator usage values. Suppose the objective of a problem is to achieve a shape-matching of a single target point. If the shape-matching term is scaled to 100.0 for the actual function value of 100.0 units (i.e., 10 displacement units) before the initial optimization iteration, the total actuator usage that is scaled to 10.0 for the actual value of 1.0 may result in the problem with more difficulties in attaining a shape error better than 1.0 displacement units, as the problem may become more sensitive to actuator usage at that point. That is apparent because the actuator and shape error terms must find a compromise at some point in the process according to the proportion of these constants. Consequently, the convergence criterion is dependent on these factors.

C. External Load Dependency and Reversibility

The solution of the preceding basic formulation is dependent on the external load, and therefore special attention should be given to the effect of external loads. The external load dependency is evident because the displacement of a structure at target points will be dependent on applied external loads, and the resulting displacements will not be the same if the loads vary or completely vanish:

$$U_j(\boldsymbol{\rho}, \boldsymbol{\rho}_A, \mathbf{F}_{\text{ext}}) \neq U_j^*(\boldsymbol{\rho}, \boldsymbol{\rho}_A) \tag{23}$$

where $\boldsymbol{\rho}$ and $\boldsymbol{\rho}_A$ are the structural and actuator partitions of design variables, respectively. The ideal scenario permits actuator variables to be varied to allow the structure to morph into desired configurations precisely as in Eq. (24), though neither reliability nor feasibility can be assured:

$$U_j(\boldsymbol{\rho}, \boldsymbol{\rho}_A, \mathbf{F}_{\text{ext}}) = U_j^*(\boldsymbol{\rho}, \boldsymbol{\rho}_A^*) \tag{24}$$

The load dependency of the solution is clearly undesirable if the structure is to be capable of morphing independently of external loads (for example, morphing when the vehicle is on the ground). Although one may argue that the solution should be obtained without applied external loads to eliminate the load-dependency issue, the consideration of these loads in the problem is indeed essential. These external loads provide a desirable problem definition that encourages structures, along with actuators, to have a capability to work against the loads. Additionally, the actuation energy can possibly be extracted from the applied external loads if they are considered in the problem. Such an energy extraction is certainly ideal, as its characterization may parallel the energy extraction from an airstream. To deal with the aforementioned problem characteristics, external load independency strategies must be incorporated in the solution process.

As the external load independency and reversibility are essential characteristics of morphing structures, the basic formulation must be modified to address these issues. In addition, there must be a requirement that the reversible structure must be stiff enough to work against external loads. The method devised in this investigation involves the introduction of an artificially defined condition that encourages the initial or reference configuration, which is one of the target configurations, to be held rigidly, thereby providing the structure with ability to work against the external loads using a few artificially placed actuators at the wing root. These actuators are determined through the optimization process and, by reversing the actuation direction, possess the ability to mimic the external loads in case these loads are diminished or vanished:

$$U_j(\boldsymbol{\rho}, \boldsymbol{\rho}_A, \mathbf{F}_{\text{ext}}) = U_j^*(\boldsymbol{\rho}, \mathbf{F}^*(\boldsymbol{\rho}^*_{\text{artificial}})) \tag{25}$$

where $\boldsymbol{\rho}^*_{\text{artificial}}$ is the control parameter that determines the use of artificial actuators, and the asterisk denotes the reversed actuation direction. The preceding condition can be replicated when the following objective function approaches zero, indicating no displacements at the morphing boundary for the reference configuration.

Minimize:

$$f_{0R}(\boldsymbol{\rho}) = \sum_{j \in \text{tgt}} \left(U(\boldsymbol{\rho}, \boldsymbol{\rho}_{\text{artificial}}, \mathbf{F}_{\text{ext}})_j^{(0)} \right)^2 \tag{26}$$

The objective function (26) replaces the zeroth or reference shape term in the original objective (1). Although one may notice that the preceding objective is nearly identical to that of the original shape term, the introduction of Eq. (26) provides a more distinct problem definition that the external loads must be handled via rigid structures using few actuators at the wing root. The sensitivity of this objective term can be obtained in the same fashion as the preceding formulation and is similar to that of the shape term in Eq. (1), in which target displacements are assigned to be zero for this case.

The reference configuration should be chosen according to the design requirement. The reasonable choice is to select the most essential configuration to be the reference. For instance, if the vehicle is to be designed to spend most of its mission duration in a certain configuration, that particular configuration should be chosen to be the reference. Though such a selection technique is certainly not a requirement, it makes the best sense, as such a reference implies the resting shape of a morphing structure and that the compliant components in the structure carry the least amount of strain at that configuration.

D. Actuator Distribution Control

The second term in the multi-objective function (1) represents the actuator usage of the system. This actuator usage is simply the sum of all the actuator variables for every configuration, which is equivalent to the sum of actuator forces in the system. Though this expression of actuator usage may be sufficient for a two-configuration system that only requires two actuator load sets, it is impractical for a multiple-configuration case due to its distribution characteristics. A simple explanation can be devised from Fig. 2. Suppose that there is a point and it must be delivered to two separate locations, as shown in Fig. 2a; the best and most efficient way, in terms of actuator usage in Eq. (1), is to use multiple force vectors that are aligned closely with the directions of motion. In fact, such an actuator distribution is probably necessary if the targets are sufficiently apart. Alternatively, if the targets are located in close proximity, the optimization shall still favor an actuator distribution for the same reason, as the optimization

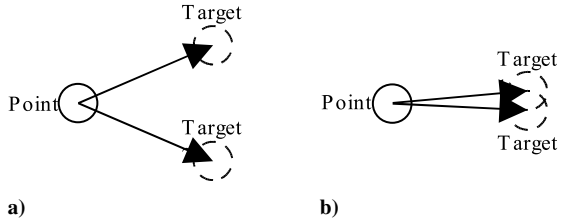

Fig. 2 Targets: a) far and b) close.

process tries to minimize the use without any consideration of the quantity of actuator locations. Although the resulting distributed actuation may be the most efficient form, excessive distribution is generally not desirable in the physical context. Therefore, the basic formulation must be modified to accommodate the actuator distribution control.

Among several methods that can be devised to control actuator distribution, the method studied in this investigation involves a modification to the actuator term in the objective function (1).

Minimize:

$$f_{0A} = W_{A1} f_{A1} + W_{A2} f_{A2} \tag{27}$$

where f_{A1} is the actuator usage term from the original formulation (1), and f_{A2} is the actuator distribution control term. The actuator distribution term is there to maximize the concentration of interconfiguration actuator variables in a single physical location, which can be expressed as the following maximizing problem.

Maximize:

$$f_{A2+} = \sum_{i=1}^{N_\Omega} \prod_{j \in \Omega_i} \rho_j \tag{28}$$

where Ω_i is the set of actuator variables at the ith physical location, and N_Ω is the maximum number of physical locations available for actuators to occupy. To solve this maximizing problem in the minimization form of Eq. (27), one well-known technique is a weighted summation form that adds a negative of the maximizing term f_{A2+} to the minimizing problem.

Minimize:

$$f_{0A} = \sum_{i=1}^{N_{\text{shape}}} W_{A1}^{(i)} \sum_{j \in A_i} \rho_j - W_{A2} \sum_{i=1}^{N_\Omega} \prod_{j \in \Omega_i} \rho_j \tag{29}$$

This actuator objective function replaces an actuator minimization term in the original objective function (1). The proportion of weight constants $W_{A1}^{(i)}$ and W_{A2} determines the magnitude of actuator distribution or concentration. One must remember that the actuator distribution control term may cause an opposing effect on the actuator usage term if it is weighted excessively. Therefore, careful consideration should be given upon choosing a weight proportion.

Another possible way to treat such contradictory terms is to use a ratio form in which minimizing and maximizing terms are placed in the numerator and denominator, respectively.

Minimize:

$$f_{0A} = \frac{\sum_{i=1}^{N_{\text{shape}}} W_{A1}^{(i)} \sum_{j \in A_i} \rho_j}{\sum_{i=1}^{N_\Omega} \prod_{j \in \Omega_i} \rho_j} \tag{30}$$

The primary disadvantage of the ratio form is that the balance between actuator distribution and use cannot be controlled, as the weight proportion is irrelevant for this case. Therefore, the weighted summation form [Eq. (29)] is the preferred technique in the investigation.

E. Modified Relative Volume Constraint

The relative volume constraint (5) in the basic formulation is a simple sum of line variables and does not represent the physical volume that can be occupied by line elements. This imprecise volume definition is primarily due to the multiple structural design variables that are assigned to a line element in any particular locations. More specifically, the root of this ill-defined volume comes from two design variables for a line element that separately control axial and bending stiffness (i.e., the $L1$ and $L2$ set of variables). A frame element that expends two units of volume instead of a unit volume for a truss or telescoping element will likely be disfavored by the optimization process. Consequently, the ideal volume definition for such a case should therefore be based on the physical existence of a line element instead of the total quantity of structural variable.

To accomplish such a task, the volume constraint can be modified to count a single unit of volume for each line element, regardless of whether it is a frame, a truss, or a telescope:

$$f_V = \sum_{i \in L1} \rho_i + \sum_{i \in L2} \rho_i - \sum_{i=1}^{N_\Phi} \prod_{j \in \Phi_i} \rho_j - V_{\max} \le 0 \tag{31}$$

where Φ_i is the set of structural variables at the ith physical location, and N_Φ corresponds to the number of available physical locations that line elements can occupy. The preceding volume constraint enhances the volume definition, as the sum-of-products term ensures that the frame usage is unbiased. One may also notice that the volume constraint becomes analogous to *or logic* as the solution approaches 0–1 design.

III. Example Problems and Results

The example problem provided here involves a three-configuration morphing wing design, including loiter (surveillance), high-lift (landing), and climb (takeoff) configurations, as shown in Fig. 3. The problem portrays the generic surveillance unmanned aerial vehicle (UAV) mission that requires the majority of its flight time in a loiter configuration. Therefore, configuration 0 or the reference configuration should be the loiter configuration that must be held rigidly using a minimum amount of artificial actuators at the wing-root section. Configuration 1 is the high-lift configuration with a large wing-planform-area increase of approximately 84%. One should notice that the motion between configurations 0 and 1 is solely an area expansion and does not involve any sweeping motions. The third configuration is the climb configuration and has a 30 deg (i.e., 15 deg with respect to the reference) sweep with a slight area increase of 14%. For the entire target shapes, the leading-edge length remains the constant, implying that the leading edge must make a rigid-body rotation around the wing root. Although such a problem definition fixes the optimization solution in a manner equivalent to the preassignment of a leading-edge spar, the explicit definition of the structural components is avoided in the investigation to observe the characteristics of the problem formulation.

The semiground structure with 4×4 cells, as shown in Fig. 1a, with evenly distributed initial design variables is selected to be the starting point in the optimization process. The structure has 72 line elements with definitions that each location can be occupied by

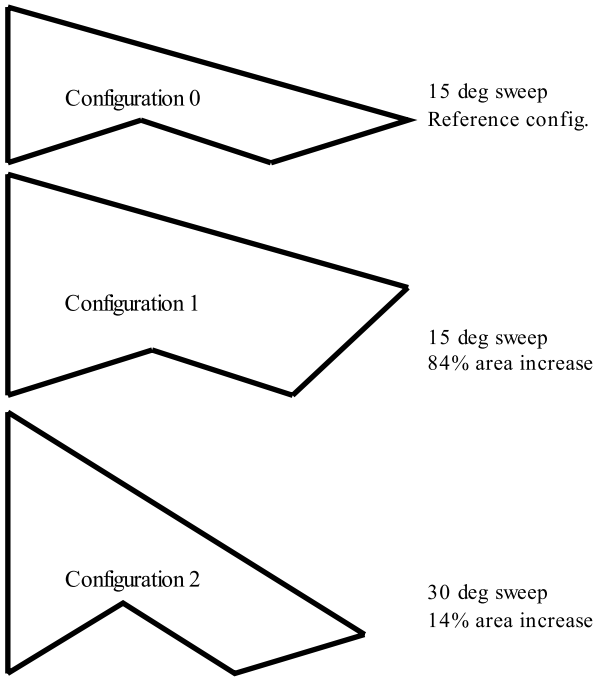

Fig. 3 Generic morphing UAV example problem.

frame, truss, telescope, or actuator elements. Among these line elements, there are 64 potential locations with 262 design variables for actuators and active telescopes. In addition, the model contains 144 joint elements and 5 potential fuselage attachments. Overall, the problem contains 555 design variables. The problem is solved using the globally convergent version of the method of moving asymptotes developed by Svanberg [21,22].

The physical dimensions of the wing are also selected to simulate the generic UAV. The reference configuration has a wingspan of 10 ft. The physical and material properties of the full frame element are chosen to resemble a frame with 1 by 1 in.^{2} cross section that is made of common aluminum alloy. The beam and truss elements are the decomposition of a full frame structure with the same physical and material properties. The maximum allowable actuator force per actuator is set to 1000 lb. To simulate the in-plane drag loads experienced during the flight, nodal forces of 100 lb are applied to four leading-edge locations, as shown in Fig. 1a. The element stroke limit is set to 15 in., regardless of its original length. The skin element has small membrane stiffness, yet it provides some resistance to relative motions and does not act as a load-bearing structure. Table 1 summarizes the input data used to solve this example problem.

A. Base Solution

The solution shown in Fig. 4 is regarded as the base solution because no actuator distribution control and modified volume control measures are applied to the problem. The total normalized shape error for the case is 0.1216, indicating that approximately 88% of the desired total target displacement is met. The highest actuator usage value (i.e., sum of actuator variables for a configuration) of 5.5367 occurs in configuration 1. The maximum useful actuator work value, which occurs in configuration 1, is $30,619$ in. $\cdot$ lb. The number represents the peak actuator energy in transition to the strain energy in flexible skin, compliant joints, and residual compliant members, and it can probably be regarded as an indication of how compliant or articulate the structure/mechanism might be.

One may notice that structural components in the solution are dominantly truss elements with 22 trusses, 7 inactive telescopes, and only 2 frames. As explained previously, this truss-dominant solution may be a resultant of the biased volume definition in Eq. (7). The leading-edge section has a rather concentrated formation of truss elements, indicating that the spar is required to resist the simulated drag loads. The structure is mainly composed of a spar at the leading edge and a combination of linkages in various orientations. The spar formation is connected to a fuselage through a pin joint, and other attachments along the wing root are sliding connections. The inactive telescopes are more prevalent in the trailing-edge section. This is probably due to the change in length of the trailing edge as the structure moves from one configuration to another.

Following the definition in the problem formulation, the optimization chose an appropriate artificial actuator to hold the reference configuration rigidly against the simulated drag loads, as clearly indicated in Fig. 4a. Configuration 1 has 8 active actuators and 2 active telescopes. Configuration 2 has 9 active actuators and an active telescope. The total number of actuator locations in the solution is 16 and they appear to be excessively distributed. In addition, it is clearly evident that the sweeping motion and root section shape are controlled mainly at the wing-root section with actuators through a mechanism that somewhat resembles a 4-bar linkage. The local shape changes seem to be accomplished by a combination of rectangular-shaped linkages and corresponding distributed actuators that are placed across the wing.

Table 1 Input parameters for the example problem

Input parameter	Value
$W_S^{(i)}$	20/70/50 for $i = 0,1,2$
$W_{A1}^{(i)}$	0.02 for all i
W_{A2}	0.01 (low), 0.02 (high)
$A^{(i)}$	10 for all i
A_T	10
α, β, p	6
$\mathbf{F}_j^0$	1000 lb for all j
$V_{\max}$	32
$E_{\max}^{(i)}$	15 in. for all i
Skin modulus and thickness	200 psi, 0.1 in.
Line cross section	1×1 in.
Line-element material	Aluminum
Initial $\boldsymbol{\rho}$, structure	0.25
Initial $\boldsymbol{\rho}$, actuator	0.01

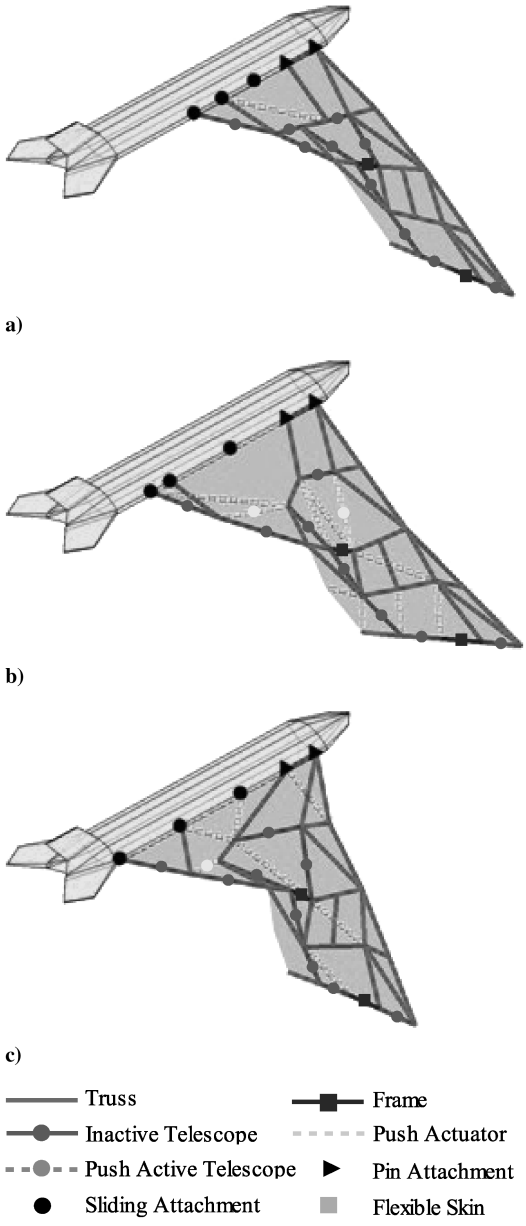

Fig. 4 Base solution for a) configuration 0, b) configuration 1, and c) configuration 2.

B. Solution with Modified Volume Constraint

The solution shown in Fig. 5 resulted from the problem with all the same parameters and conditions as in the previous case, but it has the modified volume constraint definition that does not bias frame usage. The normalized total shape error is 0.0972, which is slightly better than that of the previous case. The maximum actuator usage value of 5.4479 occurs in configuration 1 and the corresponding maximum useful actuator work is $30,919$ in. $\cdot$ lb, indicating the similarities between the current and previous cases in the actuation energy requirement and the structural compliance. Although the topology

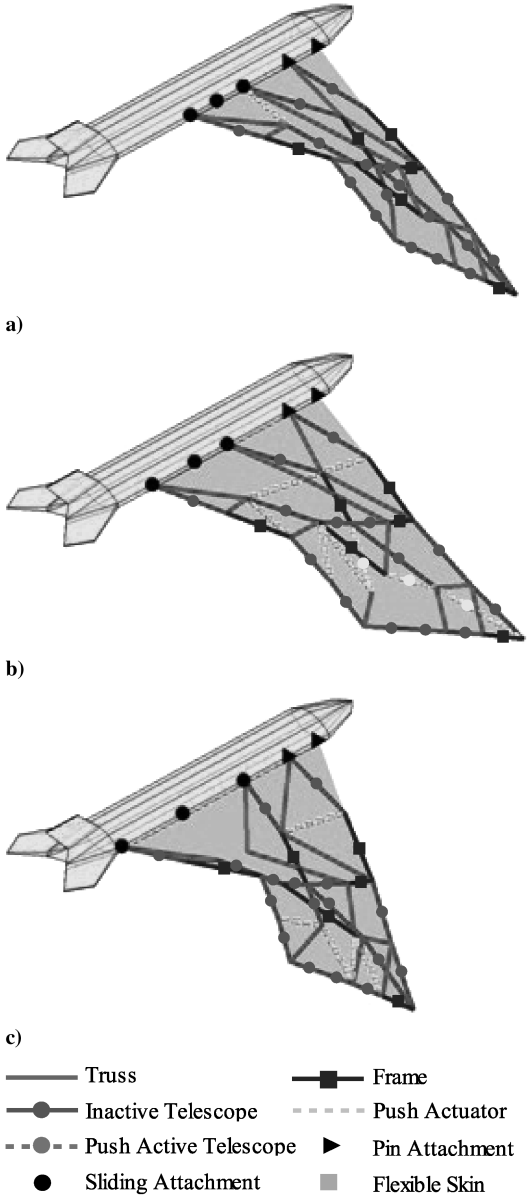

Fig. 5 Modified volume constraint solution for a) configuration 0, b) configuration 1, and c) configuration 2.

may appear to be significantly different from that of the previous case, close examinations and comparisons reveal that the fundamental characteristics of the structures are nearly identical.

In the figure, the expected effect of the modified volume constraint can be observed. It is clearly visible that the amount of frame in the solution has increased, as compared with the previous solution. The structural partition of the solution is composed of 12 trusses, 6 frames, and 13 inactive telescopes. For the same reason as the previous case, the optimization process creates a sparlike structure at the leading edge that is connected to the fuselage through a pin joint. One may notice the absence of a line element at the leading edge at the root and that the load-bearing structure is connected to the second pin joint instead of the first one. This is reasonable, because the model does not contain a simulated drag load at the root, and an independent fixed joint at the leading edge is more than capable of holding the flexible skin in position.

Similar to the previous case, the structure attains its local motions through a combination of linkages and corresponding actuators placed along the entire span. Overall, there are 3 active telescope and 14 actuator locations. Configuration 1 uses 5 active actuators and 3 active telescopes. Configuration 2 has 5 active actuators and no active telescopes. Additionally, it is worthwhile to point out that the position of active actuator and active telescopes are the only interconfiguration variations and the structural topology remains the constant over the entire configuration, as clearly indicated in the figures.

C. Actuator Distribution Control Solution with Modified Volume Constraint

Although the distributed actuation system is often considered to be energy-efficient, the excessive distribution of active elements (i.e., actuators and active telescopes) is physically impractical for numerous reasons. In fact, the actuator distributions in Figs. 4 and 5 appear to be rather excessive. To promote the concentration of actuation forces at fewer locations, the actuator distribution control strategy in Eq. (29) is applied to the problem that is identical in definitions and conditions to the previous cases.

The solution in Fig. 6 shows the favorable effect of the actuator distribution control. The total number of active element locations for the case is 8 (5 actuator and 3 active telescope locations), which is dramatically less than that of the previous cases. The total normalized shape error and the maximum actuator usage are 0.1807 and 5.2152, respectively. Though the actuator usage has improved, the shape accuracy has decreased to approximately 82%. The outcome is

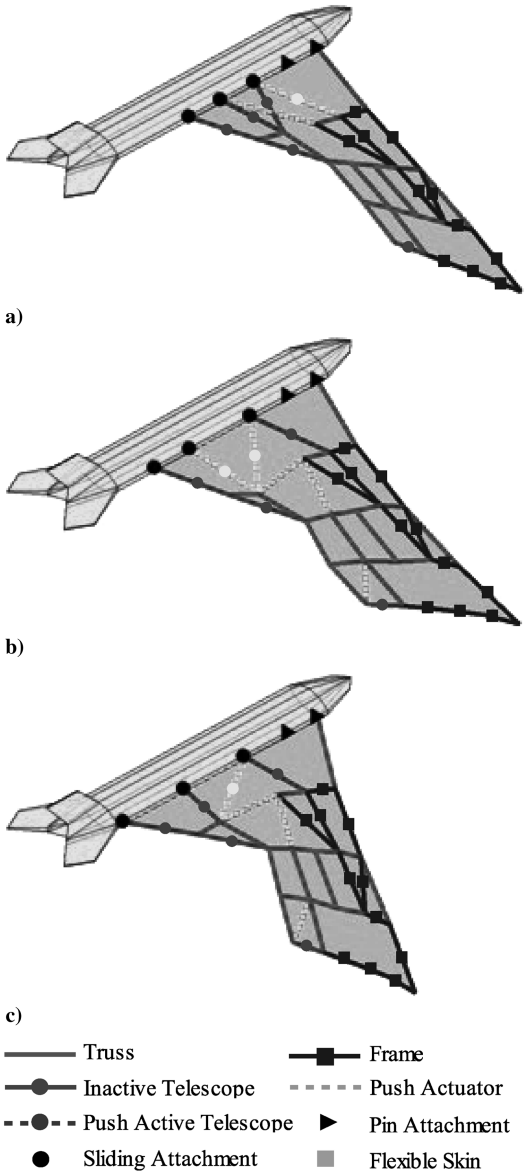

Fig. 6 Actuator distribution control solution with modified volume constraint for a) configuration 0, b) configuration 1, and c) configuration 2.

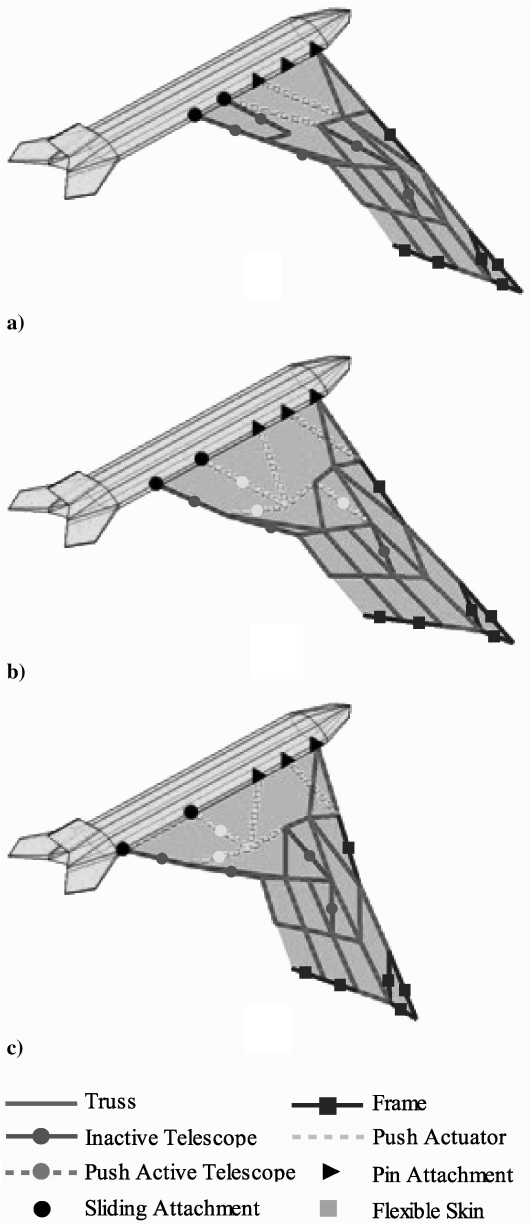

Fig. 7 Actuator distribution control solution with modified volume constraint and higher distribution control parameter for a) configuration 0, b) configuration 1, and c) configuration 2.

somewhat explicable, as the optimization has to compromise the shape objective to achieve the solution with fewer actuator locations. The structural components in the solution are composed of 16 trusses, 11 frames, and 5 inactive telescopes. Furthermore, the clear distinction between the load-bearing frame structure at the leading edge and the rectangular mechanisms can be made from the figure. The active components are 5 actuators and 3 active telescopes, with the maximum useful actuator work value of 27, 154 in. · lb. Among these locations, configuration 1 uses 4 active actuators and 2 active telescopes. Configuration 2 has 5 active actuators and an active telescope.

The actuator distribution control parameter can be further increased to possibly allow the solution with fewer actuator distributions. The solution in Fig. 7 has 7 actuator locations with the higher distribution parameter. That is not a significant reduction, but one may hypothesize that the amount of actuator distribution is necessary to meet the reasonable shape-matching objective value. The shape objective is generally weighted much heavier than the actuator objective, because it is of primary importance in the problem. For the structural part, there are 23 trusses, 6 frames, and 3 inactive telescopes. It is also noteworthy that the maximum actuator usage and the corresponding maximum usable work are 5.0111 and 21, 341 in. · lb, respectively. The lower use and work values may indicate that the solution employs less elastic motions than the previous solutions. The total normalized shape error is 0.1775, which is similar to that obtained in the case with a lower distribution parameter. Table 2 summarizes the solutions of the example problem.

IV. Conclusions

This investigation introduced a novel approach for the conceptual design of morphing wing structures through a topology optimization methodology. The primary emphasis of the investigation was to extend the fundamental formulation previously introduced by the authors to one more advanced in concept. In addition to redeveloping the formulation into one that is capable of accommodating the multiple-configuration definitions, several improvements were made in the formulation to provide more precise definitions of a structural volume and the means to control actuator distributions. The important issues on the external load dependency and the reversibility of a morphing design, as well as the appropriate selection of a reference configuration, were also addressed in the investigation.

The solution of the three-configuration example problem clearly revealed that actuator distribution control and modified volume strategies introduced in the investigation are effective and indeed improve the solution quality. The basic formulation provided a truss-dominant structure with excessive actuator distributions. This truss-dominant solution is understandable, as the original volume constraint has the tendency to bias frame usage. To reduce the truss dominance and encourage frame usage in the solution, the problem was solved with modified volume constraints. The solution clearly showed that the modified volume constraints have a favorable effect of reducing the truss dominance, though slight distortions in structural topology are visible. To provide a more reliable solution, actuator distribution control was applied to the problem. The solution showed the dramatic improvement in both structural topology and actuator distribution. It was evident that the combination of these volume and actuator distribution definitions drastically improved the solution quality and provided means to tailor a solution in accordance with design requirements. Further reduction in actuator distribution was attempted, but the optimization did not respond to the tightened actuator distribution parameter. One can hypothesize that the actuator concentration at that point had peaked and no further

Table 2 Solution comparison for the three-configuration example problems

Formulations	Quantity							
	Push actuator	Pull actuator	Active telescope	Inactive telescope	Truss	Frame	Pin/fixed attachment	Sliding attachment
Basic	14	0	2	7	22	2	2	3
Modified volume	11	0	3	13	12	6	2	3
Modified volume and low distribution control	5	0	3	5	16	11	2	3
Modified volume and high distribution control	4	0	3	3	23	6	3	2

reduction in distribution could be made without sacrificing the shape objective.

Although additional investigations are required to further refine the methodology, it was sufficiently demonstrated, via example problems, that the methodology presented in this paper may provide a valid conceptual morphing wing design. The future investigation must include dimensional aspects (i.e., shape and size) of the structure, along with out-of-plane schemes to handle aerodynamic-pressure loads and coupled aeroelastic conditions. Although numerous assumptions and simplifications were made in the investigation, it is the authors' opinion that this preliminary investigation serves as one of the important initiatives toward a successful development of a computational tool for the conceptual design of a morphing structure.

Acknowledgments

The authors acknowledge the support by Dayton Graduate Studies Institute (DAGSI) and U.S. Air Force Office of Scientific Research (AFOSR). The authors would also like to thank Krister Svanberg of the Royal Institute of Technology (KTH), Stockholm, for assistance in the method of moving asymptotes (MMA) code. The opinions and conclusions presented in the paper are those of the authors and do not necessarily reflect the views of the acknowledged individual or organizations.

References

[1] Hall, J., "Executive Summary AFTI/F-111 Mission Adaptive Wing," Wright Research Development Center, Rept. WRDC-TR-89-2083, Wright–Patterson AFB, OH, Sept. 1989.

[2] Miller, G., "Active Flexible Wing Technology," Air Force Wright Aeronautical Lab., Rept. TR-87-3096, Wright–Patterson AFB, OH, Feb. 1987.

[3] Pedersen, C. B. W., Buhl, T., and Sigmund, O., "Topology Optimization of Large Compliant Mechanism," *International Journal for Numerical Methods in Engineering*, , Vol. 50, No. 12, 2001, pp. 2683–2705. doi:10.1002/nme.148

[4] Kawamoto, A., "Path-Generation of Articulated Mechanisms by Shape and Topology Variations in Non-Linear Truss Representation," *International Journal for Numerical Methods in Engineering*, Vol. 64, No. 12, 2005, pp. 1557–1574. doi:10.1002/nme.1407

[5] Maute, K., and Reich, G., "Integrated Multidisciplinary Topology Optimization Approach to Adaptive Wing Design," *Journal of Aircraft*, Vol. 43, No. 1, 2006, pp. 253–263. doi:10.2514/1.12802

[6] Gano, S., Perez, V., Renaud, J., Batill, S., and Sanders, B., "Multilevel Variable Fidelity Optimization of a Morphing Unmanned Aerial Vehicle," 45th AIAA/ASME/ASCE/AHS/ASC Structures, Structural Dynamics and Materials Conference, AIAA Paper 2004-1763, Palm Springs, CA, 19–22 Apr. 2004.

[7] Ramrakhyani, D., Lesieutre, G., Frecker, M., and Bharti, S., "Aircraft Structural Morphing Using Tendon-Actuated Compliant Cellular Trusses," *Journal of Aircraft*, Vol. 42, No. 6, 2005, pp. 1614–1621. doi:10.2514/1.9984

[8] Bharti, S., Frecker, M., and Lesieutre, G., "Optimal Structural Design of a Morphing Wing Using Parallel Non-Dominated Sorting Genetic Algorithm II (NSGA II)," *Smart Structures and Materials Conference*, Proceedings of SPIE, SPIE6166-02, Society of Photo-Optical Instrumentation Engineers, Bellingham, WA, Mar. 2006.

[9] Maute, K., Reich, G., and Sanders, B., "In-Plane Morphing Designs by Topology Optimization," *Proceedings of the 15th International Conference on Adaptive Structures and Technologies*, DEStech, Lancaster, PA, 9–12 Oct. 2005, pp. 291–300.

[10] Inoyama, D., Sanders, B., and Joo, J., "Conceptual Design and Multidisciplinary Optimization of In-plane Morphing Wing Structures," *Smart Structures and Materials Conference*, Proceedings of SPIE, SPIE 6166-01, Society of Photo-Optical Instrumentation Engineers, Bellingham, WA, Mar. 2006.

[11] Lu, K.-J., and Kota, S., "Design of Compliant Mechanisms for Morphing Structural Shapes," *Journal of Intelligent Material Systems and Structures*, Vol. 14, No. 6, 2003, pp. 379–391. doi:10.1177/1045389X03035563

[12] Lu, K.-J., and Kota, S.,"An Effective Method of Synthesizing Compliant Adaptive Structures Using Load Path Representation," *Journal of Intelligent Material Systems and Structures*, Vol. 16, No. 4, 2005, pp. 307–317. doi:10.1177/1045389X05050104

[13] Frecker, M., "Recent Advances in Optimization of Smart Structures and Actuators," *Journal of Intelligent Material Systems and Structures*, Vol. 14, Nos. 4–5, 2003, pp. 207–216. doi:10.1177/1045389X03031062

[14] Frecker, M., Ananthasuresh, G., Nishiwaki, G., Kikuchi, N., and Kota, S.,"Topological Synthesis of Compliant Mechanism Using Multi-Criteria Optimization," *Journal of Mechanical Design*, Vol. 119, No. 2, 1997, pp. 238–245. doi:10.1115/1.2826242

[15] Austin, F., Rossi, M. J., Van Nostrand, W., and Knowles, G., "Static Shape Control for Adaptive Wings," *AIAA Journal*, Vol. 32, No. 9, 1994, pp. 1895–1901. doi:10.2514/3.12189

[16] Saxena, A., "Topology Design of Large Displacement Compliant Mechanisms with Multiple Materials and Multiple Output Ports," *Structural and Multidisciplinary Optimization*, Vol. 30, No. 6, 2005, pp. 477–490. doi:10.1007/s00158-005-0535-z

[17] Padula, S., and Kincaid, R., "Optimization Strategies for Sensor and Actuator Placement," NASA TM 199 209126, 1999.

[18] Cook, A., and Crossley, W. A., "Genetic Algorithm Approaches to Smart Actuator Placement for Aircraft Flight Control," 41st AIAA/ASME/ASCE/AHS/ASC Structures, Structural Dynamics, and Materials Conference, AIAA Paper 2000-1582, Atlanta, GA, 3–6 Apr. 2000.

[19] Joo, J., Sanders, B., Johnson, T., and Frecker, M.,"Optimal Actuator Location Within a Morphing Wing Scissor Mechanism Configuration," *Smart Structures and Materials Conference*, Proceedings of SPIE, SPIE 6166-03, Society of Photo-Optical Instrumentation Engineers, Bellingham, WA, Mar. 2006.

[20] Joo, J., Sanders, B., and Washington, G., "Energy Based Efficiency of Adaptive Structure Systems," *Smart Materials and Structures*, Vol. 15, No. 1, 2006, pp. 171–181. doi:10.1088/0964-1726/15/1/046

[21] Svanberg, K., "The Method of Moving Asymptotes—A New Method for Structural Optimization," *International Journal for Numerical Methods in Engineering*, Vol. 24, No. 2, 1987, pp. 359–373. doi:10.1002/nme.1620240207

[22] Svanberg, K., "A Globally Convergent Version of MMA Without Line Search," *Proceedings of the First World Congress of Structural and Multidisciplinary Optimization*, Pergamon, New York, 1995, pp. 9–16.